Chirality Transfer in Magnetic Coordination Complexes Monitored by Vibrational and Electronic Circular Dichroism

Tao Wu,*[a] Xiao-Peng Zhang,[a] Xiao-Zeng You,*[a] Yi-Zhi Li,[a] and Petr Bouř*[b]

Magnetic coordination complexes based on Schiff bases are promising new molecular materials for electronics. Two μ-oxo Fe[III] dimeric complexes of enantiomers of Schiff base ligands (N,N′-(1R,2R)-1,2-diphenylethylenebis(salicylideneimine) (H₂salphen-R, **1 a**) and N,N′-(1S,2S)-1,2-diphenylethylenebis(salicylideneimine) (H₂salphen-S, **1 b**)) were synthesized; further reaction with 4-salicylideneamino-1,2,4-triazole (Hsaltrz) led to enantiomers of two one-dimensional (1D) Fe[III] coordination complexes. The structures of these complexes were determined by X-ray diffraction. Magnetic susceptibility measurements revealed that μ-oxo dimeric complexes displayed strong antiferromagnetic coupling, whereas the 1D complexes exhibited paramagnetic behavior. The chirality of the Schiff bases transferred to macromolecular chirality of the complexes, which could be monitored by both vibrational and electronic circular dichroism (CD) spectroscopic methods. The macroscopic handedness was manifested in CD signals attributed to exciton coupling between the ligands. Thus, the chiral spectroscopies were useful to probe the chirality of the complexes, their structure, and the polymerization degree.

Introduction

Chirality is one of the most prominent properties of biomolecules and thus exhibits a primary role in the functioning of many living systems. It is also becoming increasingly important from a more industrial point of view, for example, in chiral coordination complexes. They can be used in many domains of chemistry, such as asymmetric catalysis, chiral recognition, chiral molecular materials, and metallosupramolecular chemistry.[1] However, chirality in coordination chemistry is still rather unexplored if compared to its role in organic and biomolecular chemistry.[2] Yet, manipulating the handedness in coordination complexes is a key for relating their potential properties and reactivity to their structure and composition.

The transfer of chirality from ligand to metal-ion center is the most efficient way to asymmetric synthesis of coordination complexes.[3] The macroscopic chirality of a complex or polymer is caused by the chiral component, which can be seen in various ways in circular dichroism (CD) spectra. For example, in the case of exciton coupling of ligand in the complex, the signal can be significantly increased or distorted if compared with the spectrum of the original chiral component. In this work, we are particularly interested in how the complexation is manifested in the spectra of coordination polymers for molecular magnets, not explored by chiral spectroscopies so far.

Molecular magnets based on coordination complexes attract considerable interest owing to the possibility to fine-tune their physical properties through versatile chemical synthesis.[4] Generally, molecular magnetism is compatible with a broad range of other physicochemical properties,[5] which is helpful for designing multifunctional materials. Particularly interesting to us is the integration of chirality and magnetism.[6] During the past few years, enantiomeric chiral magnets (ECMs) have drawn much interest from both chemists and physicists because of the forecast[7] and detection in paramagnetic[8] and diamagnetic[9] materials of a cross-effect, which appears exclusively in enantiopure magnetized systems. This combination of Faraday effects and natural CD is designated as a magnetochiral effect that is proportional to the magnetization, and its intensity was predicted to be profoundly promoted in ECMs. Therefore, it is fascinating to interpret the synergetic effects between the geometry and magnetic properties generated from manipulated chirality.

Circular dichroism spectroscopy[10] arises from the difference in absorption of left and right circularly polarized light. It includes electronic CD (ECD) seeing electronic transitions and vibrational CD (VCD) reflecting vibrational transitions. Both have been widely used as convenient methods in stereochemical analysis of organic and biomolecular systems and coordination complexes. The ECD of coordination complexes is extremely significant for monitoring the absolute configuration,[11] but

[a] Dr. T. Wu, X.-P. Zhang, Prof. X.-Z. You, Prof. Y.-Z. Li
State Key Laboratory of Coordination Chemistry
School of Chemistry and Chemical Engineering
Nanjing National Laboratory of Microstructures
Nanjing University, Nanjing 210093 (P. R. China)
Fax: (+86) 25-83314502
E-mail: twu@nju.edu.cn
youxz@nju.edu.cn

[b] Prof. P. Bouř
Institute of Organic Chemistry and Biochemistry
Academy of Sciences
Flemingovo nám. 2, 16610 Prague 6 (Czech Republic)
Fax: (+420) 224-310-177
E-mail: bour@uochb.cas.cz

the vibrational technique displays more local structural information.[12]

For coordination complexes, VCD usage is still rather limited, although latest works suggest a great potential here as well. For example, Nafie et al. successfully implemented VCD spectra of transition-metal complexes, which afforded good density functional theory (DFT) simulation compared to experimental data.[12b] Nafie also systematically analyzed the role of low-lying excited electronic states[12c] in the enhancement of VCD in these transition-metal coordination compounds. Sato et al. discussed the impact of the d-electron configurations of metal ions of tris(β-diketonato) metal complexes on the VCD shape.[13] Crassous et al. demonstrated the high sensitivity of the VCD signal of rhenium complexes for the observation of parity violation effects.[14] You et al. successfully employed VCD spectroscopy for monitoring the coordination process of transition metal to a chiral ligand.[11e] They also evidenced that the VCD technique is a powerful detector of subtle variances of chirality in small biologically active systems including metal,[15a] as well as in detecting small changes of the enantiomeric excess during the racemization process.[15b]

Establishing of suitable routines for incorporating chirality in physicochemical explorations of molecular materials is one of the ambitious goals for both chemists and physicists. Herein, we investigate the application of VCD and ECD spectroscopy to monitoring the chirality transfer in 1D iron(III) Schiff base complexes. These systems were selected because the Schiff base complexes are of considerable interest in the design of molecule-based magnetic materials, owing to the versatile geometrical modifications leading to magnetic anisotropy alternation.[16] To the best of our knowledge, this work presents the first attempt at VCD characterization of coordination polymers in solution. CD techniques offer, for example, monitoring of the exciton coupling, that is, interaction of azomethine groups conjugated with aromatic chromophores, which occurs during the polymerization.
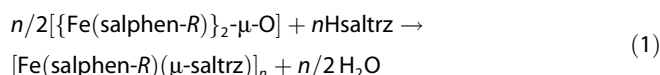
Results and Discussion

Synthesis and general characterization

Enantiomers of Schiff base ligands N,N'-(1R,2R)-1,2-diphenylethylenebis(salicylideneimine) (H$_2$salphen-R; **1a**) and N,N'-(1S,2S)-1,2-diphenylethylenebis(salicylideneimine) (H$_2$salphen-S; **1b**) were prepared by condensation reaction of chiral diamines (**1a** from the R,R configuration and **1b** from the S,S configuration) and salicylaldehyde[18a] (Scheme 1). Both enantiomers were collected as yellow crystals.

It is generally believed that Fe^{II} bis(salicylidene)ethylenediaminato (salen)-type complexes are prone to oxidation in air, which is reflected in the composition of the more stable μ-oxo Fe^{III} dimeric species.[17] The chiral bulky ligand H$_2$salphen-R was previously supposed to be unable to form a μ-oxo dimer owing to the steric repulsion of the molecular backbone compared to its *meso* geometry.[18] In addition, synthesis of the ligand with iron salts under an inert atmosphere is recommended. However, by performing the synthesis in air with sub-

sequent redissolution in dichloromethane/ethanol mixed solution, a μ-oxo Fe^{III} dimer was obtained as red blocks through slow evaporation. Normally if the reaction is performed with the participation of other monodentate Lewis bases, such as pyridine, thiolate, or chloride, a five-coordinate compound is formed.[19] Interestingly, altering the solvent from methanol to pyridine affords analogous μ-oxo Fe^{III} dimer [{Fe(salphen-R)}$_2$-μ-O]·3 Py (**2c**); its single-crystal unit incorporates three pyridine (Py) molecules.

The reaction of the μ-oxo iron(III) complex [{Fe(salphen-R)}$_2$-μ-O] (**2a**) with coligand 4-salicylideneamino-1,2,4-triazole (Hsaltrz) follows Equation (1):

$$n/2[\{\text{Fe(salphen-}R)\}_2\text{-μ-O}] + n\text{Hsaltrz} \rightarrow$$
$$[\text{Fe(salphen-}R)(\text{μ-saltrz})]_n + n/2\,\text{H}_2\text{O} \tag{1}$$

The unique crystal structure of the 1D Fe^{III} polymer **3a** incorporates one methanol molecule. The compositions of these complexes were supported by elemental analysis together with X-ray crystallographic data, and electronic and infrared absorption spectra. Note that compounds **1a** and **1b** are reported enantiomeric molecules, whereas compounds **2a**–**c**, **3a**, and **3b** are new species.

Structures of complexes and absolute configurations

Relevant crystallographic data of compounds **2** and **3** are listed in Table 1; selected bond lengths [Å] and angles [°] of complexes **2** and **3** are listed in Table S1 in the Supporting Information. The results are reasonably close to data published for similar achiral cases.[16d,18b] In the μ-oxo dimer complex, the coordination around the central iron(III) atom leads to a distorted square-pyramidal (SPY) geometry. In the achiral structure, the two *meso*-(salphen)$^{2-}$ ligand skeletons are on the same side, whereas in the optically active case they lie in opposite directions with a slight angle distortion owing to the steric hindrance. As a result, the bridge oxygen atom looks like a pseudo-center of inversion (Figure 1). A lower symmetry is achieved through the addition of a pyridine unit for complex **2c**. According to the topographical stereochemistry of the five-coordinate unit, the absolute configurations of the two iron atoms in complex **2a** are both assigned as Λ configuration.[20] Analogously, the absolute configurations of the two iron atoms in the enantiomeric complex **2b** both should be of Δ configuration.

The 1D polymer shares the zigzag chain.[16d] The coordination around the central iron(III) atom is an octahedral (OC-6) arrangement; the {FeN$_3$O$_3$} skeleton is in a facial geometry (Figure 2).[16d,20a] As a result of the sterically hindered diphenyl group, the Fe···Fe distance (9.98 Å) is much longer than in the other cases.[16d] The absolute configuration around the central iron(III) atom of the polymer **3a** is Λ.[20a] The consistent configuration manifests that the chirality transferred from the ligand to the iron(III) atom is consistent during the 1D chain complexation process.
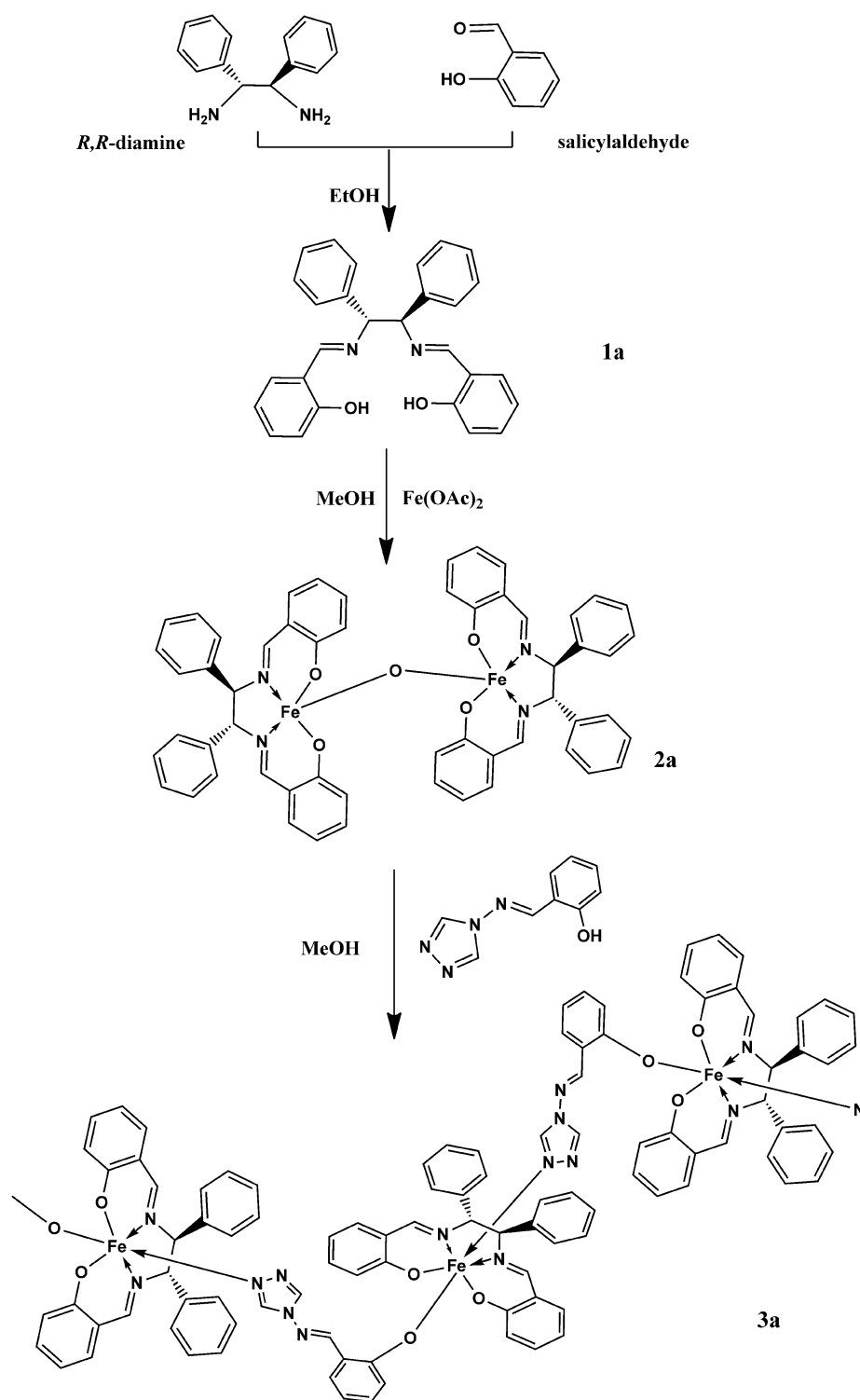
Scheme 1. Synthesis route: from chiral pool diamine to 1D iron(III) coordination polymer.

Magnetic properties

The dependencies of magnetic susceptibilities χ_M and $\chi_M T$ on the temperature for the μ-oxo dimer complex enantiomers **2a** and **2b** are almost the same (Figure 3). The difference between values of χ_M and $\chi_M T$ for the enantiomers of 1D chain complexes **3a** and **3b** are tiny as well. For complex **2a**, the value of

$\chi_M T$ is 0.945 cm^3 K mol^{-1} at 300 K and shows a clear decrease from 300 to 50 K (0.556 cm^3 K mol^{-1}), which indicates a strong antiferromagnetic coupling between the two iron(III) centers through the oxo bridge (Fe···Fe distance, 3.49 Å). For complex **3a**, the value of $\chi_M T$ is 4.238 cm^3 K mol^{-1} at 300 K and there is no distinctive value variance from 300 to 5 K (4.143 cm^3 K mol^{-1}), thus exhibiting a normal paramagnetic behavior. This indicates that there is no clear spin coupling between two iron(III) centers through the 4-salicylideneamino-1,2,4-triazolate bridge,[16d] which is reasonable for the longer Fe···Fe distance. As a result, the magnetic property of the 1D chain can be represented approximately by the magnetic behavior of each unique iron(III) center.

UV/Vis absorption and ECD spectra

As expected, the UV/Vis spectra of the enantiomers of the chiral pool diamines, the ligands (**1a** and **1b**), the μ-oxo dimer complexes (**2a** and **2b**), and 1D polymer (**3a** and **3b**) share almost the same curve, whereas their ECD spectra nearly look like mirror images (Figure 4). Although there are several differences between the crystal structures of **2a** and **2c**, there are minimal variances of the UV/Vis and ECD spectra in dichloromethane, which indicates that the conformation of the μ-oxo dimer complex in solution is very stable.

There is no outstanding chromophore in the chiral pool molecule, and only one weak absorption band around 220 nm of the substituted benzene transition is observed. The R,R-diamine corresponds to a positive Cotton effect (CE) curve, whereas the S configuration gives a negative one. In the UV/Vis spectrum of ligand **1a**, the intense bands around 230 and 258 nm are assigned to π–π* transition of the azomethine group, whereas the broad band around 320 nm is the n–π*

Table 1. Crystallographic data and structure refinement details for complexes **2** and **3**.					
	2a	**2b**	**2c**	**3a**	**3b**
formula	$C_{56}H_{44}Fe_2N_4O_5$	$C_{56}H_{44}Fe_2N_4O_5$	$C_{56}H_{44}Fe_2N_4O_5 \cdot 3(C_5H_5N)$	$C_{37}H_{29}FeN_6O_3 \cdot CH_3OH$	$C_{37}H_{29}FeN_6O_3 \cdot CH_3OH$
M_r	964.65	964.65	1201.95	693.55	693.55
T [K]	173(2)	173(2)	296(2)	296(2)	296(2)
crystal system	$P\bar{1}$	$P\bar{1}$	$P2_1$	$P2_1$	$P2_1$
space group	triclinic	triclinic	monoclinic	monoclinic	monoclinic
a [Å]	13.4093(12)	13.394(3)	12.9259(9)	9.2038(10)	9.2005(4)
b [Å]	13.6355(11)	13.629(3)	16.2575(11)	18.315(2)	18.3343(8)
c [Å]	15.1288(14)	15.108(3)	15.2354(10)	10.2439(12)	10.2483(5)
α [°]	66.600(2)	66.532(3)	90.00	90.00	90.00
β [°]	66.931(3)	66.863(3)	105.5370(10)	95.824(2)	95.8770(10)
γ [°]	85.695(2)	85.502(3)	90.00	90.00	90.00
Z	2	2	2	2	2
D_{calcd} [g cm^{-3}]	1.378	1.383	1.294	1.341	1.339
μ [mm^{-1}]	0.679	0.681	0.527	0.488	0.488
reflections measured	23 808	18 418	18 796	11 875	11 817
unique reflections (R_{int})	17 329(0.0152)	13 501(0.0437)	11 749(0.0269)	7116(0.0155)	7635(0.0152)
number of parameters	1207	1207	766	436	443
goodness-of-fit on F^2	1.178	1.004	1.008	1.071	1.047
R_1,[a] wR_2[b] [$I > 2\sigma(I)$]	0.0570, 0.1478	0.0517, 0.1402	0.0426, 0.0869	0.0327, 0.0834	0.0293, 0.0741
R_1,[a] wR_2[b] (all data)	0.0600, 0.1500	0.0600, 0.1486	0.0717, 0.0869	0.0370, 0.0862	0.0320, 0.0755
[a] $R_1 = \Sigma(|F_o| - |F_c|)/\Sigma|F_o|$. [b] $wR_2 = [\Sigma w(F_o{}^2 - F_c{}^2)^2/\Sigma w(F_o{}^2)^2]^{1/2}$.					

transition of the azomethine group.[21] The CE shape in the ECD spectrum associated with the π–π* and n–π* transitions of the azomethine chromophore is in good agreement with the R,R configuration of the diamine skeleton.[22]

As the μ-oxo dimer complex formed, these π–π* and n–π* transitions displayed a redshift. For complex **2a**, the π–π* transition moved to 241 nm, with a broad slope between 281 and 330 nm. The n–π* transition shifted to 347 nm, and was also mixed with the oxo to iron(III) charge-transfer (CT) transition.[23] The exciton coupling effect[11e, 24] of the n–π* chromophore is very large compared to that of the free ligand. It exhibits a positive peak at a longer wavelength ($\Delta\varepsilon_1$, 386 nm) and a negative peak at shorter wavelength ($\Delta\varepsilon_2$, 345 nm). The amplitude of the couplet ($\Delta\varepsilon_1 - \Delta\varepsilon_2$) is approximately up to 26 L mol^{-1} cm^{-1}.[10] The weak absorption around 460–600 nm corresponds to a salphen ligand to iron(III) CT (LMCT) transition,[11a, 23] accompanied by a very weak negative CE in the ECD spectrum.

Time-dependent DFT (TDDFT) computations supported the experimental UVCD spectra only approximately. The calculated (B3LYP/6-31G**/CPCM(dichloromethane)) spectra of the R,R-diamine, ligand **1a**, and complex **2a** are presented in Figure S4; for **1a** and complex **2a** the calculation is compared to experiment in Figure S5. By comparing Figure S4 and Figure 4 we can see that the trend observed in the spectra is well reproduced, that is, the diamine absorbs in the lowest wavelengths only, with a relatively weak CD, whereas for **1a** and **2a** the absorption threshold shifts to longer wavelengths, and the ratio of CD over absorption increases. Unfortunately, for the compound with iron (**2a**) the TDDFT method provides many unrealistic low-energy (high-wavelength) transitions and the overall agreement with the experiment is not good (Figure S5). This failure could not be improved by another functional (CAM-

B3LYP) or change of the pseudopotential, and it is probably caused by the complicated electronic structure, beyond the capabilities of available TDDFT implementations.

The geometry of the central iron(III) shifted from five-coordinate (SPY-5) to six-coordinate (OC-6) during the extension procedures of μ-oxo dimer to 1D framework. The UV/Vis spectrum of polymer **3a** has been considerably modified through the incorporation of the saltrz ligand. The π–π* transitions are around 235 nm, and two new peaks near 270 and 279 nm and a narrow slope between 290 and 317 nm appear. The n–π* transition has shifted to 334 nm, perhaps mixed with the saltrz LMCT transition. The exciton coupling effect of the n–π* chromophore on the ECD shape is almost identical to that of **2a**, that is, it also exhibits a positive peak at longer wavelength ($\Delta\varepsilon_1$, 386 nm) and a negative peak at shorter wavelength ($\Delta\varepsilon_2$, 345 nm). The amplitude of the couplet is lower (18 L mol^{-1} cm^{-1}). According to an empirical rule for the octahedral complexes,[24] this couplet is related to a Λ configuration. The ECD curves of complexes **2a** and **3a** are almost identical, so the absolute configuration at the five-coordinate iron(III) could be considered as the Λ configuration. These assignments are in agreement with the X-ray data. The region around 450–600 nm is assigned as the LMCT transition in the coordination polymer. In the corresponding ECD shape a weak couplet is detectable. The two salphen planes adopt nearly perpendicular positions in the 1D zigzag chain (Figure 2), which could probably induce this intramolecular couplet. In addition, the new saltrz LMCT transition might contribute. In the μ-oxo dimer unit, the arrangement of the two salphen plates is approximately parallel at opposite directions (Figure 1), not favorable for the exciton coupling.[11a, 24]
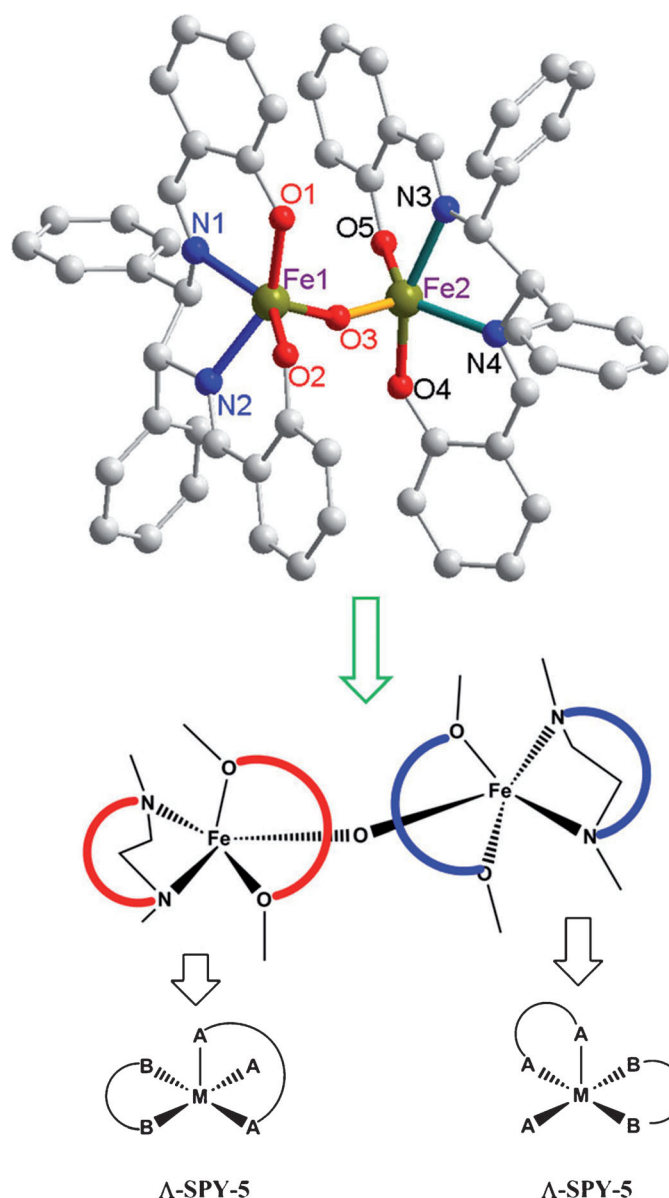
Figure 1. Crystal structure of dinuclear complex **2 a** and absolution configurations around the central iron(III) atoms. The hydrogen atoms are omitted for clarity.

Infrared and VCD spectra

The diamine provides rather weak IR and VCD spectra (Figure S6). The calculated energies and Boltzmann population of the conformers (Figure S7) in chloroform are listed in Table S2.

Three conformers of ligand **1 a** were selected through the AM1 method as well (Figure S8). The calculated energies and Boltzmann population of the conformers in chloroform are listed in Table S3. Except for the imine groups, the vibrations of the aromatic skeletons are quite weak in the spectra; therefore, two different concentrations were measured. A comparison of the experimental IR and VCD spectra of **1 a** with calculated data is made in Figure 5. The main absorption of the salphen ligand occurs at 1630 cm^{-1} (C=N stretching); other peaks are at 1582 cm^{-1} (C–C stretching of the benzyl rings), 1494,
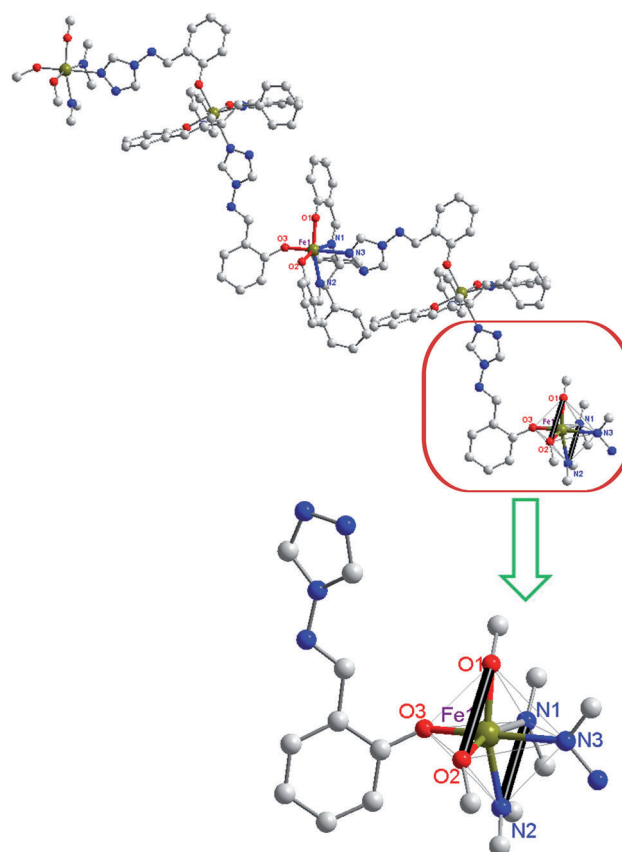

Figure 2. Part crystal structure of the zigzag 1D chain framework of coordination polymer **3 a** and the absolute configuration around the central iron-(III) atom. Solvent and hydrogen atoms are omitted for clarity.

1461, 1454, 1412, and 1382 cm^{-1} (C–H deformation), and 1278 cm^{-1} (C–O stretching). The strongest VCD peak (1454 cm^{-1}) comes from the C–H deformations of the ethylene group (based on DFT calculations), whereas the calculated most intensive peak occurs around 1656 cm^{-1}, which corresponds to the C=N stretching. Its experimental relative intensity is smaller, most probably because of uneven band broadening and the strong hydrogen-bonding interaction between the C=N bond and the –OH group, and solvation is not considered completely in the model.

Although the concentrations of both dinuclear and 1D complexes are much lower than those of the free ligand for IR and VCD measurements (Figure 6), the IR and VCD intensities are much stronger. The intensities of the dinuclear complex are even stronger than those of the 1D complex. This is explicable as the μ-oxo dimer structure is less strained than that of the polymerized chain. Most of the IR curves of **3 a** are similar to that of **2 a**, which suggests that the contribution of the saltrz molecule stretching vibrations is limited. There are no significant VCD shape changes except for intensity variances between the dinuclear geometry and the 1D chain. The results are consistent with the ECD analysis and verify that the absolute configuration at the central iron(III) atom is kept unchanged during the polymerization process. The main measured vibrational absorptions bands of **2 a** occur at: 1617 cm^{-1}
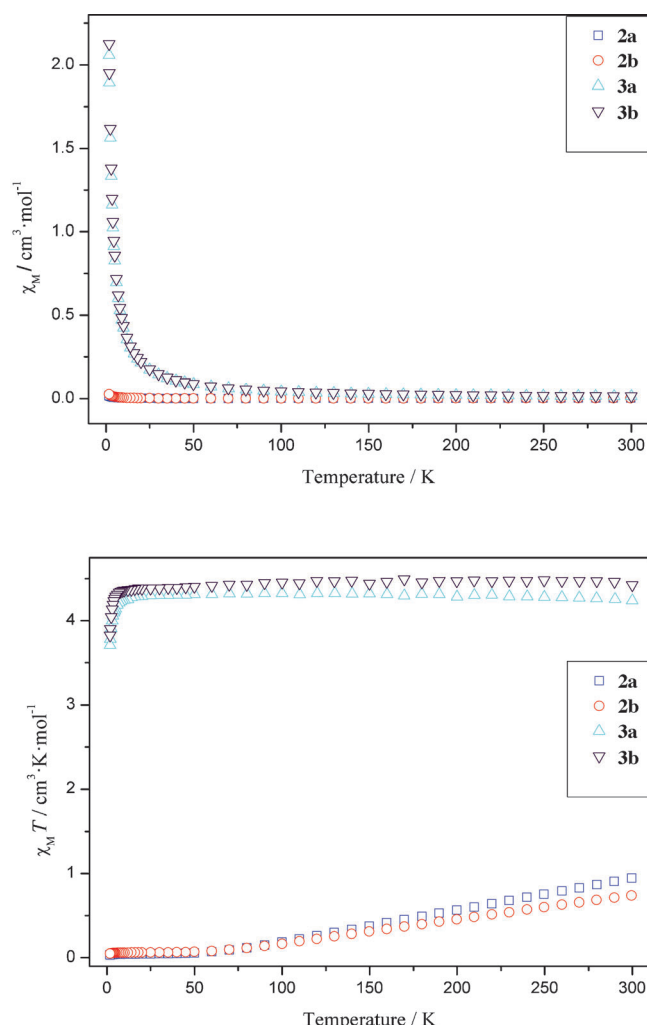
Figure 3. χ_M (top) and $\chi_M T$ (bottom) versus temperature T for complexes 2a, 2b, 3a, and 3b.

(C=N stretching); 1541 cm^{-1} (C–C stretching of the benzyl rings); and 1471, 1452, 1444, 1390, and 1342 cm^{-1} (C–H deformation). The feature IR peaks of 3a are: 1621, 1607 cm^{-1} (C=N stretching); 1543 cm^{-1} (C–C stretching of the benzyl rings); and 1470, 1454, 1445, 1390, and 1336 cm^{-1} (C–H deformation). All these vibrational bands are more intense relative to those of the free ligand. The stretching vibrations of the C–O group (1278 cm^{-1}, 1a) shifted to a higher frequency (1313 cm^{-1}, 2a; 1310 cm^{-1}, 3a) as the Fe–O bond formed.

The VCD couplet[25] of the imine chromophores in the region of 1600–1650 cm^{-1} can be detected through the whole complexation process. Comparison of measured values of $\Delta\varepsilon_1$ (lower wavenumber), $\Delta\varepsilon_2$ (higher wavenumber), anisotropy ratio g factor (also called dissymmetry factor, defined as $g = \Delta\varepsilon/\varepsilon$),[10] and the amplitude A of the couplet (defined as $\Delta\varepsilon_1 - \Delta\varepsilon_2$) of the imine groups in 1a, 2a, and 3a is made in Table 2. In addition, the C–H deformation from the phenylethylene group of the R,R-diamine is observable following the polymerization process as a tiny band

shift and a VCD peak. The measured frequency and anisotropy ratio g factors of 1a, 2a, and 3a are presented in Table 3. These increases of the anisotropy values indicate that the chirality has been effectively transferred from the ligand to the complexes, and the signal has also been amplified.

It is generally believed that VCD is less predictable for open-shell systems.[26] However, recent examples manifest that the magnetic field perturbation theory for VCD calculation can be extended to open-shell systems.[11d,e, 13] Simulations for IR and VCD spectra of complex 2a with three different exchange-correlation functionals were performed (Figure 7). The OPBE and B3PW91 functionals reproduced the IR spectra quite well (e.g., C–C stretching of the benzyl rings, observed 1543 cm^{-1}; OPBE, 1556, 1558 cm^{-1}; B3PW91, 1583, 1586, 1588 cm^{-1}), whereas the B3LYP functional provided more reasonable VCD shape simulation (e.g., C–H deformations of the ethylene group, observed 1454 cm^{-1}; B3LYP, 1495, 1497 cm^{-1}).

For the simulations of the 1D polymer 3a, monomer and dimer models were considered (Figures S9 and S10). The experimental and theoretical (except for OPBE) spectra of the dimer and monomer are very similar (Figures 8 and 9). This suggests that the chirality comes from the chiral arrangement around the central iron ion, that is, one monomeric unit. A comparison of selected IR chromophore absorptions around the central iron(III) atom measured in comparison with calculations for 1a, 2a, and 3a are presented in Table 4. As expected, the calculated frequency differences of these feature bands between 2a and the two models of 3a are quite small, which coincides with the experimental spectra.

Conclusion

By employing the 4-salicylideneamino-1,2,4-triazolate anion as bridge, the µ-oxo dinuclear complexes were successfully converted to 1D iron(III) coordination complex enantiomers. Both enantiomers of µ-oxo dinuclear iron(III) complexes with optically active bulky salen-type ligands were obtained. All these structures and absolute configurations were verified by X-ray

Table 2. VCD couplet by imine groups for 1a (0.04 M), 2a (0.015 M), and 3a (0.015 M) (see Figure 6).

	$\Delta\varepsilon_1/\nu$ (L mol^{-1} cm^{-1}/cm^{-1})	$g_1 = \Delta\varepsilon_1/\varepsilon_1$	$\Delta\varepsilon_2/\nu$ (L mol^{-1} cm^{-1}/cm^{-1})	$g_2 = \Delta\varepsilon_2/\varepsilon_2$	$A = \Delta\varepsilon_1 - \Delta\varepsilon_2$
1a	0.034/1628	2.75×10^{-5}	−0.033/1634	3.57×10^{-5}	0.067
2a	0.232/1608	8.98×10^{-5}	−0.214/1625	1.03×10^{-4}	0.446
3a	0.036/1606	1.88×10^{-5}	−0.087/1618	5.76×10^{-5}	0.123

Table 3. VCD peak by C–H deformation of phenylethylene group for R,R-diamine (0.24 M), 1a (0.24 M), 2a (0.015 M), and 3a (0.015 M; see Figure 6).

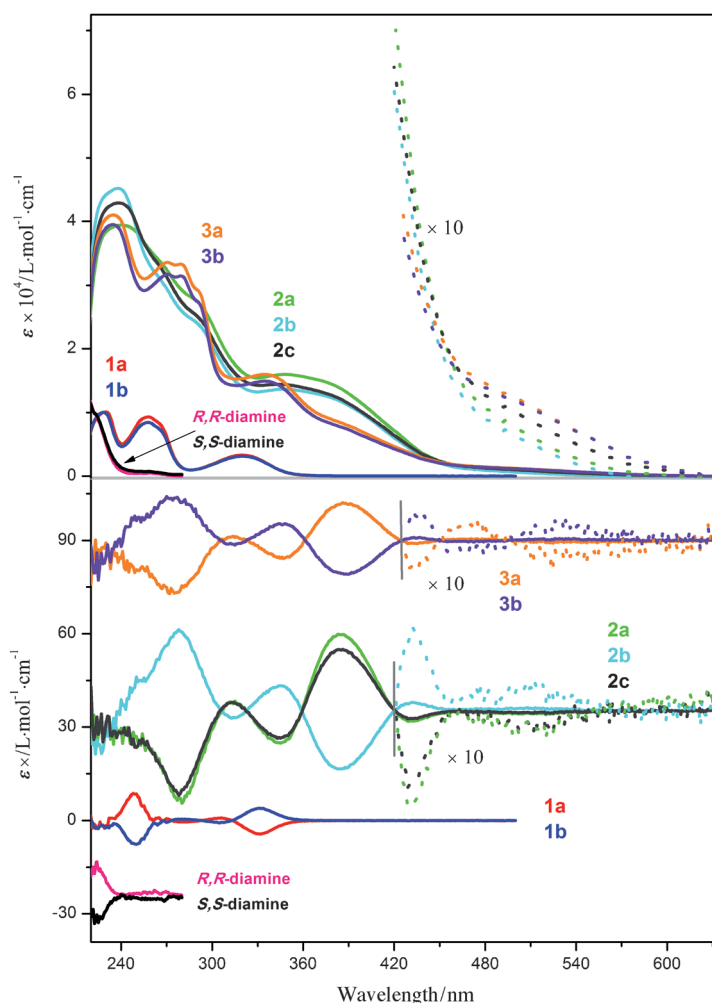| C–H deformations (phenylethylene group)	Frequency	Anisotropy
R,R-diamine	1451	8.19×10^{-5}
1a	1453	2.50×10^{-5}
2a	1454	3.46×10^{-4}
3a	1455	2.39×10^{-4}

Figure 4. UV/Vis absorption (top) and ECD (bottom) spectra of chiral pool diamines, ligand **1**, dimer complex **2**, and 1D coordination polymer **3** measured in dichloromethane solution (the concentration of all samples was kept at 6×10^{-4} M).

Table 4. Selected experimental IR peaks of the salphen part in comparison with simulations for **1 a**, **2 a**, and **3 a**.

	Experimental frequency	B3LYP functional	B3PW91 functional	OPBE functional
C=N stretching				
1 a	1634, 1628	1676, 1659	–	–
2 a	1625, 1608	1699, 1676, 1667, 1642	1692, 1683, 1679, 1671	1630, 1621, 1620,1614
3 a	1618, 1606	1686, 1677[a] 1678, 1675, 1673, 1672[b]	1700, 1691[a] 1693, 1689, 1686,1685[b]	1642, 1629[a] 1634, 1633, 1629, 1624[b]
C—O stretching				
1 a	1278	1300, 1299	–	–
2 a	1313	1391, 1378, 1356, 1336	1380, 1375, 1374, 1371	1360, 1358, 1356, 1353
[a] Monomer model. [b] Dimer model.				

crystallographic analysis. These complexes provided interesting magnetic properties and exhibited a strong chirality, both in the ECD and VCD spectra. The similarity of CD spectra between

the μ-oxo dinuclear complex **2 a** and 1D complex **3 a** confirmed the consistency of the Λ absolute configuration at the central iron(III) atom. The observed spectral behavior was partially explained by DFT modeling. This first VCD report on coordination polymers in solution indicates that, in addition to ECD, VCD spectroscopy is also a useful chiroptical technique to monitor the polymerization process. It provided information about the absolute configuration. In addition, both the electronic and vibrational chirality is magnified by the regular arrangement of the chromophores (azomethine groups, n–π* transition in ECD and C≡N stretching in VCD) enabling the strong exciton coupling.

Experimental Section

General procedures

Elemental analyses for C, H, and N were performed on an Elementar Vario Micro analyzer. Electronic absorption spectra were measured on a UV-3600 spectrophotometer in the region of 200–800 nm. ECD spectra were recorded on a Jasco J-810 spectropolarimeter in the region of 200–800 nm. IR and VCD spectra were investigated in the region of 1800–800 cm^{-1} with a VERTEX 80v Fourier transform infrared spectrometer equipped with a PMA 50 VCD/IRRAS module (Bruker, Germany) by using previous procedures.[15] The photoelastic modulator was set to 1500 cm^{-1}, the spectral resolution was 4 cm^{-1}, and the zero filling factor was 4. A demountable cuvette A145 with KBr windows with a 0.12 or 0.21 mm Teflon spacer was used. All solution samples were dissolved in deuterated chloroform. All VCD measurements were collected for 4 h composed of 12 blocks in 20 min. Baseline correction was performed with the spectra of $CDCl_3$ by using the same measurement setup as for VCD. Magnetic susceptibilities for crystalline samples were obtained on a Quantum Design MPMS-SQUID-VSM magnetometer in the temperature range of 1.8–300 K. Diamagnetic corrections were calculated using Pascal's constants.

All chemicals were purchased from commercial sources, were of analytical reagent grade, and were used without further purification. Enantiomers of Schiff base ligands (N,N'-(1R,2R)-1,2-diphenylethylenebis(salicylideneimine) (H_2salphen-R, **1 a**) and N,N'-(1S,2S)-1,2-diphenylethylenebis(salicylideneimine) (H_2salphen-S, **1 b**)) were prepared from chiral pool diamine and salicylaldehyde in dried ethanol by following procedures described elsewhere.[18a] Bridge ligand 4-(salicylideneamino)-1,2,4-triazole (Hsaltrz) was prepared from 4-amino-4H-1,2,4-triazole and salicylaldehyde in dried methanol according to conditions described elsewhere.[16d]

Syntheses

Dinuclear iron(III) complexes [{Fe(salphen)}$_2$-μ-O] **2 a** and **2 b**: The ligand H_2salphen-R (**1 a**, 84.2 mg, 0.2 mmol) was suspended in freshly dried methanol (20 mL) at room temperature, under a protective nitrogen atmosphere, and Fe(OAc)$_2$ (35 mg, 0.2 mmol, 1 equiv) dissolved in freshly dried MeOH (10 mL) was added to the ligand suspension. The mixture was stirred for 6 h under reflux. After cooling to room temperature, the resulting solution was con-
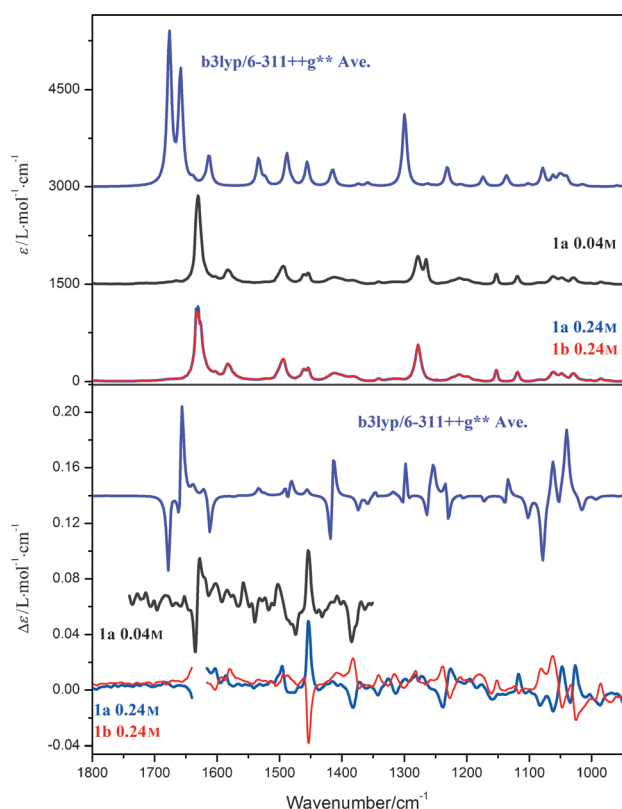
Figure 5. IR (top) and VCD (bottom) spectra of **1a** measured in CDCl₃ in comparison with DFT simulations.

centrated in vacuo, the residue was extracted with dichloromethane then washed with water in air, and the organic phase was dried over anhydrous NaSO₄ and diluted with ethanol. The red solution was left undisturbed to slowly evaporate. After several days, red crystals of [{Fe(salphen-*R*)}₂-μ-O] (**2a**) suitable for X-ray crystallography were collected (43 mg, 44.6%). Elemental analysis calcd (%) for $C_{56}H_{44}Fe_2N_4O_5$: C 69.72, H 4.60, N 5.81; found: C 69.60, H 4.67, N 5.66. Enantiomer complex [{Fe(salphen-*S*)}₂-μ-O] (**2b**) was synthesized under the same conditions with ligand H₂salphen-*S* (**1b**), and was obtained as red crystals. Elemental analysis calcd (%) for $C_{56}H_{44}Fe_2N_4O_5$: C 69.72, H 4.60, N 5.81; found: C 69.13, H 4.67, N 5.61.

Dinuclear iron(III) complexes [{Fe(salphen-*R*)}₂-μ-O]·3Py, **2c**: The ligand H₂salphen-*R* (**1a**, 84.2 mg, 0.2 mmol) was dissolved in pyridine (20 mL), then Fe(OAc)₂ (35 mg, 0.2 mmol, 1 equiv) was added to the ligand suspension under a nitrogen atmosphere. The mixture was stirred for 6 h at 70°C. The cooled red solution was then filtered in air and left undisturbed to slowly evaporate. After several days, red needle-shaped crystals of [{Fe(salphen-*R*)}₂-μ-O]·3Py (**2c**) suitable for X-ray crystallography were collected. Elemental analysis calcd (%) for $C_{56}H_{44}Fe_2N_4O_5 \cdot (C_5H_5N)_3$: C 69.72, H 4.60, N 5.81; found: C 69.54, H 4.74, N 5.77 (sample dried in vacuo for 12 h to remove pyridine).

1D iron(III) complexes [Fe(salphen)(μ-saltrz)]·CH₃OH **3a** and **3b**: Ligand Hsaltrz (62 mg, 0.33 mmol) dissolved in freshly dried methanol (5 mL) was added to a suspension (25 mL) of [{Fe(salphen-*R*)}₂-μ-O] (**2a**; 145 mg, 0.15 mmol) in freshly dried methanol. The red solution was heated for 6 h under reflux. The resulting solution was filtered and was left undisturbed to slowly evaporate. Black crystals of 1D complex [Fe(salphen-*R*)(μ-saltrz)]·CH₃OH (**3a**) suitable
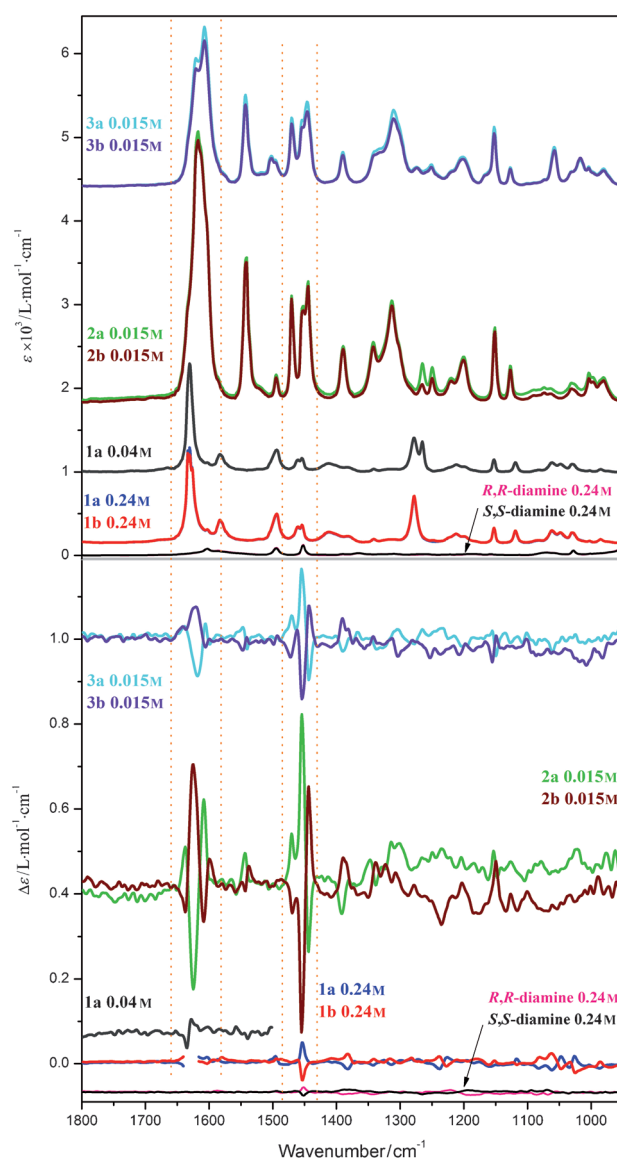

Figure 6. IR (top) and VCD (bottom) spectra monitoring the polymerization process: chirality-poor diamines, ligand **1**, dinuclear coordination complex **2**, and 1D coordination polymer **3**.

for X-ray analysis were collected after several days (123 mg, 59%). Elemental analysis calcd (%) for $C_{37}H_{29}FeN_6O_3 \cdot CH_3OH$: C 65.81, H 4.80, N 12.12; found: 65.55, H 4.89, N 11.90 (sample dried in vacuo for 12 h to remove methanol). Enantiomer 1D complex [Fe(salphen-*R*)(μ-saltrz)]·CH₃OH (**3b**) was synthesized under the same conditions with dinuclear complex enantiomer [{Fe(salphen-*S*)}₂-μ-O] (**2b**) and was obtained as black crystals. Elemental analysis calcd (%) for $C_{37}H_{29}FeN_6O_3 \cdot CH_3OH$: C 65.81, H 4.80, N 12.12; found: C 65.85, H 5.05, N 11.69 (sample dried in vacuo for 12 h to remove methanol).

X-ray crystallography

Single-crystal X-ray diffraction measurements of **2a**, **2b**, **2c**, **3a**, and **3b** were performed on a Bruker SMART APEX CCD-based diffractometer operating at room temperature. Intensities were collected with graphite-monochromatized MoKα radiation ($\lambda = 0.71073$ Å) operating at 50 kV and 30 mA, using the $\omega/2\theta$ scan
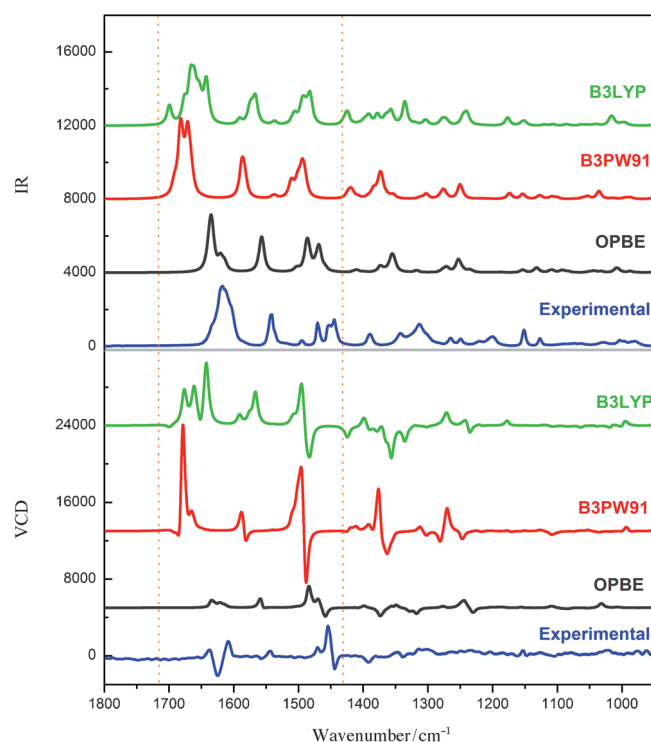
Figure 7. Measured IR (top) and VCD (bottom) spectra of complex **2 a** in comparison with theoretical calculations.

Figure 8. Measured IR (top) and VCD (bottom) spectra of complex **3 a** in comparison with theoretical calculations of monomer model.

Figure 9. Measured IR (top) and VCD (bottom) spectra of complex **3 a** in comparison with theoretical calculations of dimer model.

mode. Data reduction was made with the Bruker SAINT package.[27] Absorption corrections were performed using the SADABS program.[28] The structures were solved by direct methods and refined on F^2 by full-matrix least-squares using SHELXL-97 with anisotropic displacement parameters for all non-hydrogen atoms in all structures. All hydrogen atoms of **2 a**, **2 b**, **2 c**, **3 a**, and **3 b** were found in differential maps of electron density and their parameters were refined by using the riding model with the C—H distance of 0.95 (CH) and 0.99 (CH$_2$) Å, respectively, and with U_{iso}(H) = 1.2 U_{eq}(C). All computations were performed using the SHELXTL-97 program package.[29] Details of the crystal parameters, data collection, and refinement of complexes **2 a**, **2 b**, **2 c**, **3 a**, and **3 b** are summarized in Table 1. CCDC 970062, 970063, 970064, 970065, and 970066 contain the supplementary crystallographic data for this paper. These data can be obtained free of charge from The Cambridge Crystallographic Data Centre via www.ccdc.cam.ac.uk/data_request/cif.

Computational methods

The calculations were performed with Gaussian 09 programs.[30] The conformational search of *R,R*-diamine and **1 a** were done with the AM1 method. The lowest-energy conformers were optimized at the B3LYP level with the 6-311 + + G (d,p) basis set. The effect of the solvent was modeled by the conductor-like polarizable continuum model (CPCM) for chloroform. The calculated energies are listed in Tables S2 and S3, and the correlated structures are exhibited in Figures S6 and S7. IR and VCD spectra calculations were performed under the same conditions.

For complexes **2 a** and **3 a**, both the optimization and the calculations of IR and VCD spectra were performed under the OBPE/B3PW91/B3LYP functional combined with the LANL2DZ basis set and effective core potential (ECP) for Fe^{III} and 6-31G** for other
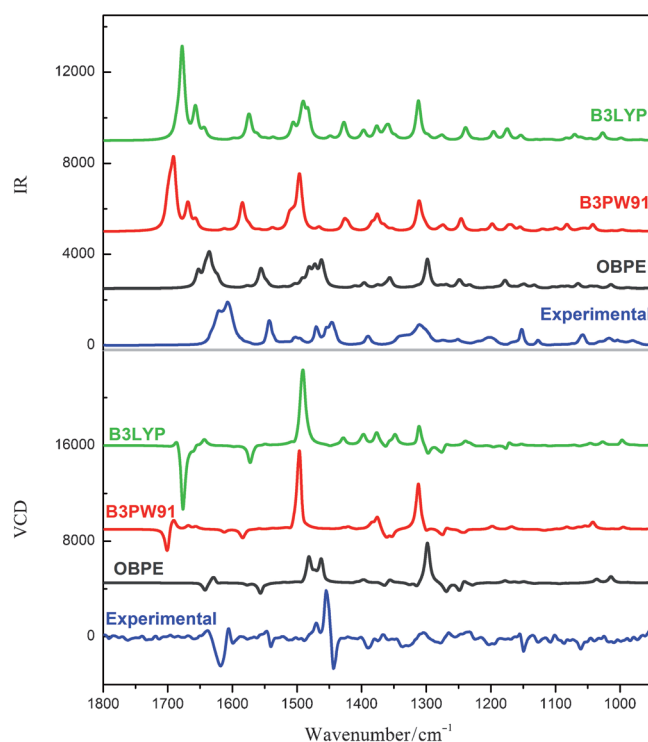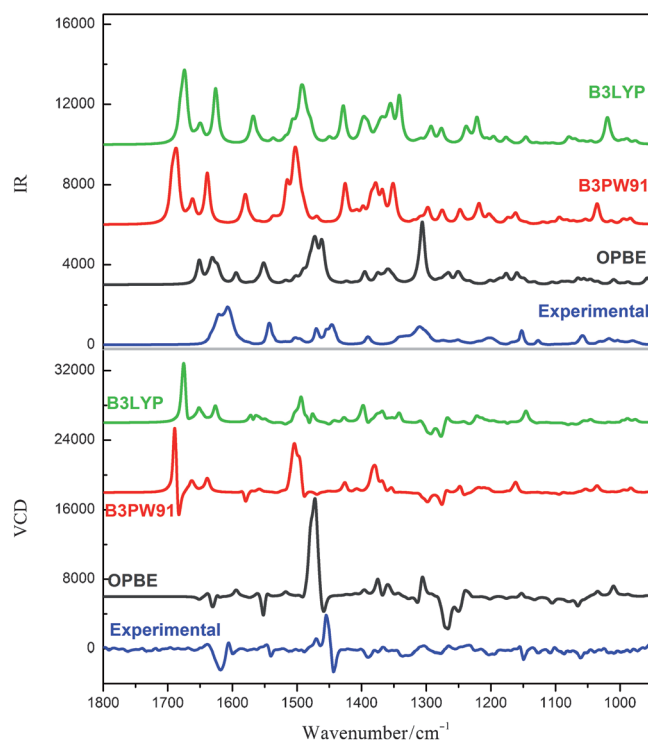
atoms. Starting geometries of the **2 a** and **3 a** models were generated from crystal structures (Figures S9 and S10). The effect of the solvent was modeled by the CPCM dielectric model as for the monomer. IR and VCD spectra calculations were performed under the same conditions.

UV/Vis and ECD spectra were simulated at the B3LYP level with the 6-31G(d,p) basis set for *R,R*-diamine and ligand **1a** (only the most populated conformations were considered), and the LANL2DZ basis set for complex **2a**. The effect of the solvent was modeled by the CPCM model for dichloromethane.

Acknowledgements

[1] a) E. B. Bauer, *Chem. Soc. Rev.* **2012**, *41*, 3153–3167; b) H. Miyake, H. Tsukube, *Chem. Soc. Rev.* **2012**, *41*, 6977–6991; c) W. Zhang, R. G. Xiong, *Chem. Rev.* **2012**, *112*, 1163–1195; d) S. E. Howson, A. Bolhuis, V. Brabec, G. J. Clarkson, J. Malina, A. Rodger, P. Scott, *Nat. Chem.* **2012**, *4*, 31–36.

[2] a) E. L. Eliel, S. H. Wilen, L. N. Mander, *Stereochemistry of Organic Compounds*, Wiley, New York, **1994**; b) W. J. Lough, I. W. Wainer, *Chirality in Natural and Applied Science*, Blackwell Science Ltd, Oxford, **2002**; c) *Comprehensive Chirality* (Eds.: H. Yamamoto, E. M. Carreira), Elsevier Science, New York, **2012**; d) E. Yashima, K. Maeda, T. Nishimura, *Chem. Eur. J.* **2004**, *10*, 42–51.

[3] a) U. Knof, A. von Zelewsky, *Angew. Chem.* **1999**, *111*, 312–333; *Angew. Chem. Int. Ed.* **1999**, *38*, 302–322; b) J. Crassous, *Chem. Soc. Rev.* **2009**, *38*, 830–845; c) J. Crassous, *Chem. Commun.* **2012**, *48*, 9684–9692; d) C. Train, M. Gruselle, M. Verdaguer, *Chem. Soc. Rev.* **2011**, *40*, 3297–3312.

[4] a) P. G. Lacroix, I. Malfant, J. Real, V. Rodriguez, *Eur. J. Inorg. Chem.* **2013**, 615–627; b) J. S. Miller, *Chem. Soc. Rev.* **2011**, *40*, 3266–3296; c) D. F. Weng, Z. M. Wang, S. Gao, *Chem. Soc. Rev.* **2011**, *40*, 3157–3181.

[5] a) E. Coronado, J. R. Galan-Mascaros, C. J. Gomez-Garcia, V. Laukhin, *Nature* **2000**, *408*, 447–449; b) S. I. Ohkoshi, H. Tokoro, T. Matsuda, H. Takahashi, H. Irie, H. Hashimoto, *Angew. Chem.* **2007**, *119*, 3302–3305; *Angew. Chem. Int. Ed.* **2007**, *46*, 3238–3241; c) E. Pardo, C. Train, H. B. Liu, L. Chamoreau, B. Dkhil, K. Boubekeur, F. Lloret, K. Nakatani, H. Tokoro, S. I. Ohkoshi, M. Verdaguer, *Angew. Chem.* **2012**, *124*, 8481–8485; *Angew. Chem. Int. Ed.* **2012**, *51*, 8356–8360.

[6] a) L. D. Barron, *Nat. Mater.* **2008**, *7*, 691–692; b) C. Train, R. Gheorghe, V. Krstic, L. M. Chamoreau, N. S. Ovanesyan, G. Rikken, M. Gruselle, M. Verdaguer, *Nat. Mater.* **2008**, *7*, 729–734.

[7] a) G. Wagnière, A. Meier, *Chem. Phys. Lett.* **1982**, *93*, 78–81; b) L. D. Barron, J. Vrbancich, *Mol. Phys.* **1984**, *51*, 715–730.

[8] a) G. L. J. A. Rikken, E. Raupach, *Nature* **1997**, *390*, 493–494; b) G. L. J. A. Rikken, E. Raupach, *Phys. Rev. E* **1998**, *58*, 5081–5084.

[9] P. Kleindienst, G. H. Wagniere, *Chem. Phys. Lett.* **1998**, *288*, 89–97.

[10] *Circular Dichroism, Principles and Applications, 2nd ed.* (Eds.: N. Berova, K. Nakanishi, R. W. Woody), Wiley, New York, **2000**.

[11] a) M. Ziegler, A. von Zelewsky, *Coord. Chem. Rev.* **1998**, *177*, 257–300; b) J. Autschbach, L. Nitsch-Velasquez, M. Rudolph, *Top. Curr. Chem.* **2011**, *298*, 1–98; c) F. J. Coughlin, K. D. Oyler, R. A., Jr. Pascal, S. Bernhard, *Inorg. Chem.* **2008**, *47*, 974–979; d) T. Wu, C. H. Li, Y. Z. Li, Z. G. Zhang, X. Z. You, *Dalton Trans.* **2010**, *39*, 3227–3232; e) T. Wu, X. P. Zhang, C. H. Li, Bouř, P. Y. Z. Li, X. Z. You, *Chirality* **2012**, *24*, 451–458; f) F. Di Salvo, M. Y. Tsang, F. Teixidor, C. Viñas, J. G. Planas, J. Crassous, N. Vanthuyne, N. Aliaga-Alcalde, E. Ruiz, G. Coquerel, S. Clevers, V. Dupray, D. Choquesillo-Lazarte, M. E. Light, M. B. Hursthouse, *Chem. Eur. J.* **2014**, *20*, 1081–1090.

[12] a) P. J. Stephens, F. J. Devlin, J. R. Cheeseman, *VCD Spectroscopy for Organic Chemists*, CRC Press, Boca Raton, **2012**; b) Y. He, X. Cao, L. A. Nafie, T. B. Freedman, *J. Am. Chem. Soc.* **2001**, *123*, 11320–11321; c) L. A. Nafie, *J. Phys. Chem. A* **2004**, *108*, 7222–7231.

[13] a) H. Sato, T. Taniguchi, A. Nakahashi, K. Monde, A. Yamagishi, *Inorg. Chem.* **2007**, *46*, 6755–6766; b) H. Sato, Y. Mori, Y. Fukuda, A. Yamagishi, *Inorg. Chem.* **2009**, *48*, 4354–4361; c) H. Sato, A. Yamagishi, *Int. J. Mol. Sci.* **2013**, *14*, 964–978.

[14] a) P. R. Lassen, L. Guy, I. Karame, T. Roisnel, N. Vanthuyne, C. Roussel, X. Cao, R. Lombardi, J. Crassous, T. B. Freedman, L. A. Nafie, *Inorg. Chem.* **2006**, *45*, 10230–10239; b) F. De Montigny, L. Guy, G. Pilet, N. Vanthuyne, C. Roussel, R. Lombardi, T. B. Freedman, L. A. Nafie, J. Crassous, *Chem. Commun.* **2009**, 4841–4843; c) N. Saleh, S. Zrig, T. Roisnel, L. Guy, R. Bast, T. Saue, B. Darquie, J. Crassous, *Phys. Chem. Chem. Phys.* **2013**, *15*, 10952–10959.

[15] a) T. Wu, C. H. Li, X. Z. You, *Vib. Spectrosc.* **2012**, *63*, 451–459; b) T. Wu, X. P. Zhang, X. Z. You, *RSC Adv.* **2013**, *3*, 26047–26051.

[16] a) M. Andruh, *Chem. Commun.* **2011**, *47*, 3025–3042; b) M. A. Halcrow, *Chem. Soc. Rev.* **2011**, *40*, 4119–4142; c) P. Herchel, Z. Šindelář, Z. Trávníček, R. Zbořil, J. Vančo, *Dalton Trans.* **2009**, 9870–9880; d) R. Herchel, L. Paveleka, Z. Trávníček, *Dalton Trans.* **2011**, *40*, 11896–11903; e) R. Ishikawa, B. K. Breedlove, M. Yamashita, *Eur. J. Inorg. Chem.* **2013**, 716–719.

[17] a) M. Gerloch, E. D. McKenzie, A. D. C. Towl, *Nature* **1968**, *220*, 906–907; b) R. G. Wollmann, D. N. Hendrickson, *Inorg. Chem.* **1978**, *17*, 926–930; c) D. J. Darensbourg, C. G. Ortiz, D. R. Billodeaux, *Inorg. Chim. Acta* **2004**, *357*, 2143–2419.

[18] a) K. Oyaizu, E. Tsuchida, *Inorg. Chim. Acta* **2003**, *355*, 414–419; b) L. N. Rusere, T. Shalumova, J. M. Tanski, L. A. Tyler, *Polyhedron* **2009**, *28*, 3804–3810.

[19] a) G. M. Bancroft, A. G. Maddock, R. P. Randl, *J. Chem. Soc. A* **1968**, 2939–2944; b) R. N. Mukherjee, A. J. Abrahamson, G. S. Paterson, T. D. P. Stack, R. H. Holm, *Inorg. Chem.* **1988**, *27*, 2137–2144; c) W. Chiang, D. Vanengen, M. E. Thompson, *Polyhedron* **1996**, *15*, 2369–2376.

[20] a) A. von Zelewsky, *Stereochemistry of Coordination Compounds*, Wiley, Chichester, **1996**; b) A. Lennartson, M. Håkansson, *Angew. Chem.* **2009**, *121*, 5983–5985; *Angew. Chem. Int. Ed.* **2009**, *48*, 5869–5871.

[21] K. K. Bania, G. V. Karunakar, K. Goutham, R. C. Deka, *Inorg. Chem.* **2013**, *52*, 8017–8029.

[22] A. Pasini, M. Gullotti, R. Ugo, *J. Chem. Soc. Dalton Trans.* **1977**, 346–356.

[23] a) J. Sanders-Loehr, W. D. Wheeler, A. K. Shiemke, B. A. Averill, T. M. Loehr, *J. Am. Chem. Soc.* **1989**, *111*, 8084–8093; b) M. Villagrán, J. Costamagna, S. A. Moya, *Transition Met. Chem.* **1997**, *22*, 22–26.

[24] S. G. Telfer, T. M. McLean, M. R. Waterland, *Dalton Trans.* **2011**, *40*, 3097–3108.

[25] a) T. Taniguchi, K. Monde, *J. Am. Chem. Soc.* **2012**, *134*, 3695–3698; b) T. Wu, X. Z. You, *J. Phys. Chem. A* **2012**, *116*, 8959–8964.

[26] a) J. R. Cheeseman, M. J. Frisch, F. J. Devlin, P. J. Stephens, *Chem. Phys. Lett.* **1996**, *252*, 211–220; b) P. J. Stephens, *J. Phys. Chem.* **1985**, *89*, 748–752.

[27] *SAINT*-Plus, version 6.02, Bruker Analytical X-ray System: Madison, WI, **1999**.

[28] GM. Sheldrick, *SADABS*. An empirical absorption correction program, Bruker Analytical X-ray Systems: Madison, WI, **1996**.

[29] GM. Sheldrick, *SHELXTL*-97, Universität of Göttingen, Göttingen (Germany), **1997**.

[30] M. J. Frisch, G. W. Trucks, H. B. Schlegel, G. E. Scuseria, M. A. Robb, J. R. Cheeseman, G. Scalmani, V. Barone, B. Mennucci, G. A. Petersson, H. Nakatsuji, M. Caricato, X. Li, H. P. Hratchian, A. F. Izmaylov, J. Bloino, G. Zheng, J. L. Sonnenberg, M. Hada, M. Ehara, K. Toyota, R. Fukuda, J. Hasegawa, M. Ishida, T. Nakajima, Y. Honda, O. Kitao, H. Nakai, T. Vreven, J. A., Jr., Montgomery, J. E. Peralta, F. Ogliaro, M. Bearpark, J. J. Heyd, E. Brothers, K. N. Kudin, V. N. Staroverov, R. Kobayashi, J. Normand, K. Raghavachari, A. Rendell, J. C. Burant, S. S. Iyengar, J. Tom asi, M. Cossi, N. Rega, J. M. Millam, M. Klene, J. E. Knox, J. B. Cross, V. Bakken, C. Adamo, J. Jaramillo, R. Gomperts, R. E. Stratmann, O. Yazyev, A. J. Austin, R. Cammi, C. Pomelli, J. W. Ochterski, R. L. Martin, K. Morokuma, V. G. Zakrzewski, G. A. Voth, P. Salvador, J. J. Dannenberg, S. Dapprich, A. D. Daniels, O. Farkas, J. B. Foresman, J. V. Ortiz, J. Cioslowski, D. J. Fox, Gaussian 09, Revision A.02, Gaussian, Inc., Wallingford, CT, **2009**.